Laser propagation analysis using Plexiglas™ burn samples

John S. Foley
United Technologies Industrial Lasers
Market Development (Retired)
52 Trebbe Drive
Manchester, Connecticut 06040

Sallie S. Townsend, MEMBER SPIE
University of Hartford
College of Engineering, Technology and Architecture
200 Bloomfield Avenue
West Hartford, Connecticut 06117
E-mail: ltownsend@hartford.edu

Abstract. A method is developed to determine the propagation characteristics of a high power laser beam using only Plexiglas™ burn patterns. Under the assumption of an embedded Gaussian in the laser beam and using *ABCD* ray analysis, the fundamental laser beam characteristics, independent of the optical array, are determined. The method can be used to approximate the beam irradiance profile, peak irradiance, and beam characteristic size along the beam path, the cavity induced curvature applied to the beam, and the laser beam Rayleigh range. Finally, the beam far-field spreading angle and beam quality relative to an ideal beam are calculated. The method developed defines gross characteristics of aberrated beams generated by both stable and unstable laser designs. © *2010 Society of Photo-Optical Instrumentation Engineers.* [DOI: 10.1117/1.3400738]

Subject terms: laser; laser optics; beam quality; beam propagation; beam measurement.

Paper 090607R received Aug. 28, 2009; revised manuscript received Feb. 22, 2010; accepted for publication Feb. 26, 2010; published online Apr. 28, 2010.

1 Plexiglas™ Burn Pattern Analysis

A 2 Mod SM series 14-kW CO_2 unstable resonator laser at United Technologies Industrial Lasers[1] (UTIL, South Windsor, Connecticut) was used to generate laser burn patterns in Plexiglas™. Figure 1(a) shows a typical burn contour made in a $4\times4\times3/8$ in. block of Plexiglas™ at a distance of two meters from the laser platform at 14-kW laser power for one second. The burn contour outlines the nominal two-inch-diam laser beam, and the test taken this close to the laser image plane shows the top-hat irradiance profile for the $M=2$ unstable optical cavity. The variation in the depth of penetration is highlighted by the shadows created by the burn profile shown in Fig. 1(b). The depth of vaporized material at short burn times is typically shallow, and in this sample the maximum penetration of the laser burn profile into the Plexiglas™ is 2 mm.

It is a premise of the analysis in this work that the extent and depth of the material vaporized from the Plexiglas™ is determined by the material energy density threshold (J/cm^2) required for vaporization. The longer the burn time, the larger the volume/weight of material vaporized, with the variation in the diameter and depth of the burn contour limited by the material energy density threshold (J/cm^2) required for vaporization. Figure 2 is an illustration of the vaporization profile of a Plexiglas™ burn, and shows the parameters of importance to this study.

The profile of the burn area is a contour of constant energy density. Of special interest in this work are the irradiance I_r at the edge of the burn/no burn area, and the irradiance I_0, the center point of deepest penetration. The irradiance I_r is the irradiance of the laser beam at this radial distance from the laser beam axis, represented by I_0. Since the energy density and burn time around the edge of the burn/no burn contour are constant, the irradiance I_r is also constant. In addition, the diameter d represents the maximum diameter across the burn profile at the irradiance I_r. In this study the laser beam parameters and analysis are based on the maximum diameter across the Plexiglas™ burn/no burn contour, as measured by millimeter ruler.

The method to determine the laser beam quantitative characteristics begins with measuring the weight loss in the Plexiglas™ samples exposed to the laser. The weight loss in test samples of 4×4 Plexiglas™ blocks as a function of laser burn time from 0.3 to 2.0 sec with the laser operating at 14 kW is shown in Table 1 and Fig. 3.

The laser exposure time is controlled by a high speed shutter with a 10 msec response time, which is the time required to fully open or close the extracavity shutter. The weight of the Plexiglas™ blocks before and after being exposed to the laser was measured by laboratory equipment, with accuracy certified to greater than one milligram. The laser test station is located 12 m from the laser platform with no intervening optics. At laser burn times used in this analysis, the laser beam did not burn through the

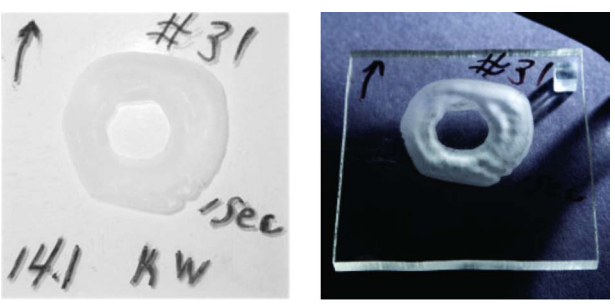

(a) (b)

Fig. 1 (a) Laser burn sample #31. (b) Highlight of burn contour.

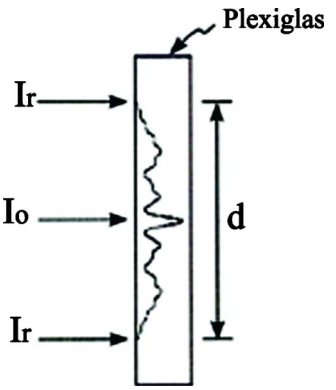

Fig. 2 Sample of Plexiglas burn/no burn profile highlighting characteristic of interest.

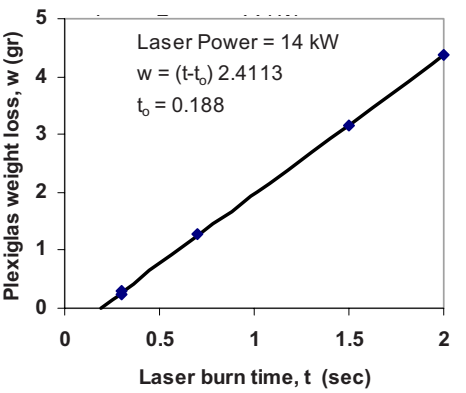

Fig. 3 Plexiglas weight loss from exposure to 14 kW of laser power.

Plexiglas™ test blocks. Therefore, all the laser energy used in vaporization of the Plexiglas™ block is captured in the measured weight loss.

The weight loss in Fig. 3 is linear, showing a loss of 2.41 g/sec burn time, and at 14 kW showing a specific energy of 5.8 kJ to vaporize one gram of Plexiglas™. The linear characteristic of the weight loss indicates that vaporization process itself is independent of the burn time, and the extent of the burn contour is determined by material threshold energy density. The vaporization process in Plexiglas™ is endothermic, which is linear. If the laser energy source is removed, the vaporization process stops. The intercept time (t_0) for zero weight loss is 0.188 sec and the correlation r^2 is 0.99. The intercept time is the critical time required to initiate vaporization at the peak laser irradiance I_0 (W/cm^2) at this location 12 m from the laser platform. The product of the peak irradiance and the intercept time ($I_0 t_0$) is a measure of the energy density threshold in the Plexiglas™. This result means that the intercept time t_0 is inversely proportional to the peak irradiance and therefore will vary with the beam power level, beam quality, and optical path distance from the laser source. Since the threshold energy density is a material characteristic, the burn pattern for each test sample and burn time extends radially out from the beam axis to the edge of the burn/no burn contour to the Plexiglas™ energy density threshold, such that:

$$I_0 t_0 = I_{r_1} t_{r_1} = I_{r_2} t_{r_2} = I_r t_r, \tag{1}$$

where, for example, the subscript r_1 is the extent of the vaporized material around the edge of the burn/no burn contour in the Plexiglas™ burn sample for a burn time of t_1 sec to irradiance I_{r_1}. For longer times, for example t_2, the vaporized pattern extends over a larger area of the Plexiglas™ test sample. The burn pattern extends to the material threshold energy density ($I_2 t_2 = I_0 t_0$). As the burn time increases, the burn pattern extends out to the wings of the beam irradiance profile limited by the energy density threshold. Therefore, the laser beam irradiance relative to the peak irradiance around the burn/no burn contour in the burn sample is given by:

$$I_r / I_0 = t_0 / t_r. \tag{2}$$

The laser burn time t_r required to vaporize the Plexiglas™ to a given radius or diameter is given by:

$$t_r = I_0 t_0 / I_r. \tag{3}$$

The required laser burn time is a function of the Plexiglas™ vaporization energy density and the laser irradiance I_r radially out from the laser beam axis, the distance r to the burn/no burn boundary.

Therefore, the energy absorbed by the Plexiglas™ is proportional to the extent of the beam burn/no burn diameter, with the irradiance at the edge of the profile being constant. For this study an equivalent Gaussian beam embedded in the propagating laser beam is assumed.[2–4] This requires that the collimated beam Fresnel number N_c of the laser beam and Gaussian be equal.[2]

$$N_c = (\pi \varpi^2)/(\lambda z) = r^2/(\lambda z). \tag{4}$$

The equivalence between the beam size radius of a laser beam (r) and a Gaussian (ϖ) is given by:

$$r^2 = \pi \varpi^2 = (d_s/2)^2, \tag{5}$$

where d_s is the beam size diameter of the propagated laser beam.

Table 1 Plexiglas™ burn data weight loss from laser burn.

Burn time (sec)	Weight before laser burn (grams)	Weight after laser burn (grams)	Weight loss (grams)	Laser burn max diameter (mm)
0.3	37.266	37.037	0.229	73
0.3	38.546	38.256	0.290	73
0.7	38.821	37.549	1.272	80
1.5	37.056	33.903	3.153	85
2.0	38.155	33.785	4.370	87

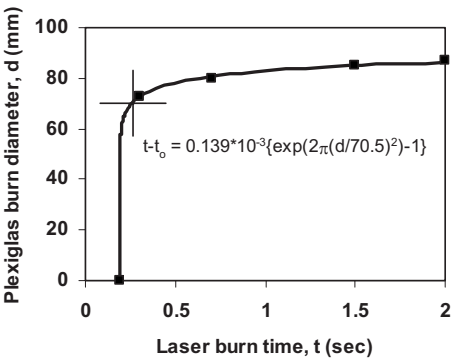

Fig. 4 Plexiglas maximum burn/no burn diameter vs. burn time.

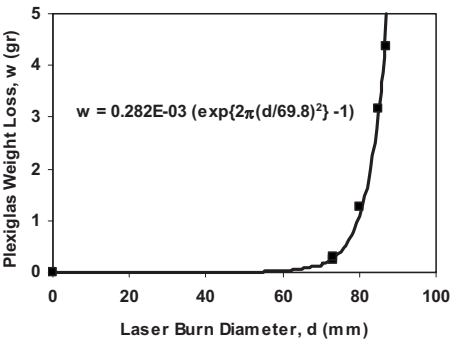

Fig. 5 Plexiglas weight loss vs. burn/no burn diameter.

The laser irradiance I_r required in Eq. (3), assuming an embedded Gaussian, is given by:[4]

$$I_r = ([2P]/[\pi\omega^2])(\exp[-2\{r/\omega\}^2]). \quad (6)$$

Substituting the laser irradiance I_r from Eq. (6) and the laser beam size d_s from Eq. (5), the required laser beam time t_r for a burn diameter d is given by:

$$t_r = ([I_0 t_0 d_s^2]/[8P])(\exp[2\pi\{d/d_s\}^2]), \quad (7)$$

and

$$t_r - t_0 = ([I_0 t_0 d_s^2]/[8P])(\exp[2\pi\{d/d_s\}^2] - 1). \quad (8)$$

The factor $([I_0 t_0 d_s^2]/[8P])$ is a constant and independent of the burn time. It is a measure of the energy intensity required to initiate and sustain vaporization in the Plexiglas™. Therefore, the regression equation used in the analysis of the Plexiglas™ burn data in this work is given by:

$$(t_r - t_0) = a(\exp[2\pi\{d/d_s^2\}] - 1), \quad (9)$$

where a is the scale factor with the dimension of time (Joules/watt) that reflects the energy absorbed by the Plexiglas™, and d_s is the laser beam size that normalizes this exponential function. The Gaussian beam size is defined as the diameter of the beam that contains 86.5% of the power. For a propagated laser beam, characteristic of the $M=2$ laser cavity, the beam size includes 80 to 90% of the power, depending on the beam Fresnel number.[2] The 80 to 90% beam power radius of this embedded Gaussian follows the same propagation laws as that of the non-Gaussian beam, such as the beam from an unstable laser resonator. Equation (9) is a key find of this work.

1.1 *Application of Theory*

Equation (9) reflects the irradiance I_r of the laser beam around the burn/no burn edge of the Plexiglas™ at burn time t_r. This equation can be used to analyze the beam size variation around the burn/no burn pattern in the Plexiglas™. This study is limited to an analysis of the maximum beam diameter etched in the Plexiglas™. The correlation of the burn/no burn diameter with laser burn time is shown in Fig. 4. The test data consist of the Plexiglas™ maximum burn/no burn diameters from Table 1 and the calculated intercept time t_0 from Fig. 3. The correlation results show a beam size d_s of 70.5 mm, a scale factor a of 0.139 msec, and correlation coefficient r^2 of 0.99.

Implicit in this analysis is the assumption that Eq. (9) also represents the energy absorbed by the Plexiglas™ around the edge of the burn/no burn contour. To demonstrate the validity of this assumption, the Plexiglas™ weight loss was correlated as a function of the laser burn diameters in Table 1, as shown in Fig. 5.

The correlation results in a scale factor of 0.28 mg and the characteristic beam size of 69.8 mm with correlation coefficient r^2 of 0.99. The difference between the two estimates of the characteristic beam size using burn time or weight loss is 0.7 mm, which is a difference of less than one percent. This result is expected because of the linear correlation between weight loss and laser burn time. In this study, further development of laser beam analysis is based on the burn time characteristics, because using weight loss ignores the unique insight gained by the time required to initiate vaporization.

The laser burn time at the characteristic beam size from the correlation in Fig. 3 is 0.262 sec. The difference between this time and t_0 is 0.074 sec of burn time. The implication of this small difference in burn time and the assumption of an embedded Gaussian is that this method of analysis will not give the fine detail of the beam irradiance profile near the peak irradiance, but will give detailed information about beam size and the tail of the irradiance profile. The irradiance profile of a laser beam can be very irregular around the peak irradiance, especially in the near field, due to diffraction effects alone (see Ref. 4, page 721).

An approximation to the laser beam irradiance profile is determined by combining Eqs. (2) and (9) and solving for I_r/I_0, as given by Eq. (10), and as shown in Fig. 6. This figure proves the exponential decay of the propagating laser beam.

The irradiance profile is a function of the Plexiglas™ burn form factor (a/t_0) and the normalized beam diameter (d/d_s).

$$I_r/I_0 = 1/(1 + \{a/t_0\}\{\exp[2\pi(d/d_s)^2] - 1\}). \quad (10)$$

At the characteristic beam size, the beam irradiance can be seen to be 71.7% of the peak value. Beyond this point, the irradiance profile continues to fall off exponentially and is virtually zero at about 1.4 times the characteristic beam

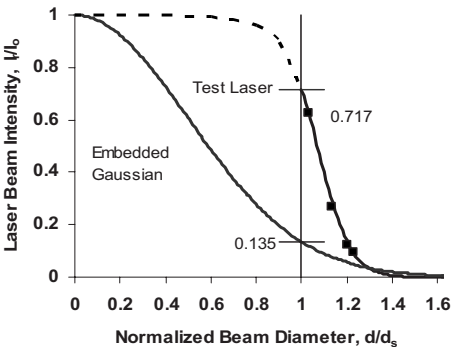

Fig. 6 Laser beam irradiance profile vs. normalized beam diameter.

size. Shown for comparison is the irradiance profile of the embedded Gaussian beam, with 13.5% of its peak irradiance at its characteristic beam size.

The peak irradiance I_0 is calculated by integrating under the effective irradiance profile. Using Eqs. (2) and (9) and assuming that the beam is circular, the analytical solution is given by Eq. (11):

$$P = \pi \int_0^{\infty} I_r r dr \quad \text{leads to} \quad I_0 = [4P(1 - a/t_0)]/[r_s^2 \ln(t_0/a)]. \tag{11}$$

Using the data from Fig. 4 (P=14E3 W, a=0.139E−3 s, t_0=0.188 s, and r_s=35 mm), the peak irradiance of the laser beam, at 12 m from the laser platform, is approximately 634 W/cm^2. The product of the peak irradiance I_0 and intercept time t_0 gives the Plexiglas™ threshold energy density for vaporization of approximately 117 J/cm^2.

The power encircled at a given radial distance of the beam is determined by integrating the beam irradiance profile [Eq. (10)], as shown in Fig. 7 and given by Eq. (12).

$$P_r/P = \{1/\ln(t_0/a)\}\{[\ln(I_r/I_0)][\exp\{2\pi(d/d_s)^2\}]\}. \tag{12}$$

Shown for comparison is the power profile of the embedded Gaussian beam, with 86.5% of its power within the characteristic beam size compared to 82.5% for the test laser. The two power profiles cross at about 1.06 diam and

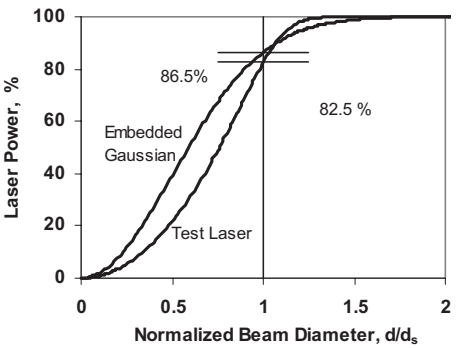

Fig. 7 Laser beam encircled power profile vs. normalized beam diameter.

by 1.25 diam the test laser beam includes 99% of the beam power. The Gaussian includes 99% power at 1.52 diam over the nominal beam size.

The test laser beam diameter that includes 99% of the total power is given by:

$$(d/d_s)_{99} = (\{1/(2\pi)\}\{\ln[\{1 - a/t_0\}/\{p_{99} - a/t_0\}]\})^{1/2}, \tag{13}$$

where

$$p_{99} = \exp[-0.99 \ln(t_0/a)]. \tag{14}$$

In summary, qualitative and quantitative data of high power laser beam characteristics can be measured from Plexiglas™ burn samples. The analysis in this work assumes a Gaussian beam embedded in the laser beam, and that the depth and extent of the material vaporized from the Plexiglas™ test sample is determined by the material energy density threshold required for vaporization. The laser beam characteristics that can be determined include the characteristic beam size, beam irradiance, and encircled power profiles. In addition, the peak power irradiance and test material energy density required for vaporization and beam diameter containing 99% of the beam power can be estimated.

2 Laser Beam Propagation Analysis

The previous section demonstrated a method to determine laser beam characteristics at a particular optical system location. This section develops a method to collapse the data from different optical configurations into a single line to recover the fundamental characteristics of the laser beam, such as beam diameter at the laser aperture, cavity-induced curvature, and Rayleigh range. The following analysis complements but does not rely on the results of the laser burn analysis in the first section. However, as in the first section, the method assumes an embedded Gaussian beam in the test laser, and that the real beam propagation path can be analyzed by an *ABCD* optical system matrix.[5] A convenient way to analyze a laser's optical system is to use *ABCD* arrays (see Ref. 5 for details). A light ray can be represented by its height h and slope h', and it is propagated by an *ABCD* array:

$$\begin{pmatrix} h_2 \\ n_2 h_2' \end{pmatrix} = \begin{pmatrix} A & B \\ C & D \end{pmatrix} \begin{pmatrix} h_1 \\ n_1 h_1' \end{pmatrix}. \tag{15}$$

The index of refraction n is included to become an optical slope. It is assumed to be unity in all that follows. Two arrays of interest here are

$$T = \begin{pmatrix} 1 & \frac{L}{n} \\ 0 & 1 \end{pmatrix} \quad \text{and} \quad R = \begin{pmatrix} 1 & 0 \\ -\frac{1}{f} & 1 \end{pmatrix}, \tag{16}$$

where T represents propagation in a medium of index n for a distance L. R represents refraction through a lens. In modeling optical systems, it is normal to replace mirrors by their equivalent lens. A multielement optical system is modeled by multiplying these matrices together in the appropriate order to determine the system *ABCD* array. In the paraxial approximation, the *ABCD* array is used to create

the end-to-end propagation integral to take the laser beam from the beginning of an optical system to its end. The United Technologies Industrial Lasers (UTIL) laser is an example of an unstable resonator, as defined in Ref. 4, chapters 15.3, 21.3, and 22. In Figs. 14 and 15 in Ref. 2, it was shown that even unstable resonator beams contain an embedded Gaussian, which tracks 85 to 95% of the encircled power, independent of Fresnel number.

As shown in Eq. (26.5) in Ref. 2, the laser beam diameter d variation through an arbitrary $ABCD$ matrix can be given by:

$$(d/d_0)^2 = A^2 + (B/Z_R)^2. \tag{17}$$

In Eq. (17), d_0 is the beam diameter at the laser aperture output, and Z_R is the laser Rayleigh range. Equation (17) assumes collimated input and traces the path of a beam ray d_0 starting at the beam aperture as it propagates through an $ABCD$ array. We address the issue of the real beam contours shortly. The ideal beam array to trace through Eq. (17) is a series of beam characteristic sizes (d_s) defined by Eq. (9) for variations along the beam path. For this analysis, the laser beam propagation path assumes a collimated laser with a cavity-induced beam output curvature $(1/f_0)$, followed by the $ABCD$ optical path matrix. As shown in Eq. (18), the total optical magnification is modified by the laser-induced curvature $1/f_0$.

$$\begin{pmatrix} A & B \\ C & D \end{pmatrix}_{\text{total}} = \begin{pmatrix} A & B \\ C & D \end{pmatrix}_{\text{external}} \begin{pmatrix} 1 & 0 \\ -1/f_0 & 1 \end{pmatrix}_{\text{internal}} = \begin{pmatrix} A - B/f_0 & B \\ C - B/f_0 & D \end{pmatrix}_{\text{total}}. \tag{18}$$

Substituting the A and B factors from Eq. (18) into Eq. (17) gives:

$$(d/d_0)^2 = (A - B/f_0)^2 + (B/Z_R)^2 = A^2 - 2AB/f_0 + (B/f_0)^2 + (B/Z_R)^2. \tag{19}$$

Dividing each side of Eq. (19) by the beam magnification A^2 and solving for the beam diameter d gives:

$$(d/A)^2 = d_0^2 - [(2d_0^2/f_0)(B/A)] + [(d_0/f_0)^2 + (d_0/Z_R)^2][B/A]^2. \tag{20}$$

The resultant equation is a quadratic in the optical beam diameter (d/A) and optical distance (B/A) with coefficients that define primary beam characteristics. The first term defines the beam diameter at the laser output aperture, the second term defines the impact of the laser-induced beam curvature, and the third term defines the beam far-field spreading angle. In turn, the far-field spreading angle is composed of two terms showing the contribution of the beam-induced curvature $(d_0/f_0)^2$ and beam diffraction $(d_0/Z_R)^2$. The laser cavity-induced curvature term has been referred to in the literature as the "correctable divergence" of the beam.[6]

Normalizing the beam diameter d and the matrix element B of the $ABCD$ array by the optical magnification A and including the induced curvature $1/f_0$ in the optical train thus creating a collimated input beam, allows test data from different external optical configurations to be collapsed into one dataset to determine the basic propagation characteristics of the collimated laser output beam. Equation (20) is a key find of this work and is shown to be valid experimentally.

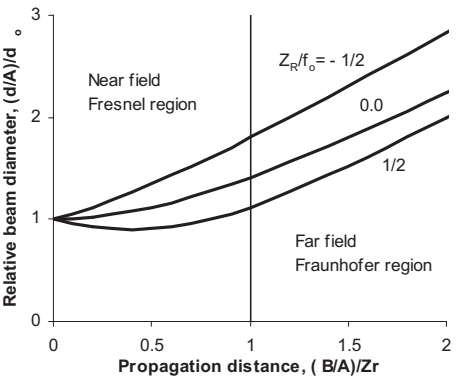

Fig. 8 Theoretical plot of relative beam diameter vs. propagation distance.

Required for proper analysis of the beam is a wide range of A and B values to cover both the near- and far-field optics range of both d/A and B/A. Including the laser-induced curvature means that the resultant quadratic gives accurate analysis of the beam propagation from both sides of the beam waist. This correlation of optics configuration gives wide latitude to determine the optimal optical configuration for a given application.

Figure 8 is a theoretical plot of the relative beam optical diameter versus propagation optical distance for three different laser cavity-induced curvatures on the beam. Figure 8 is obtained by normalizing Eq. (20) with reference to the laser aperture beam size d_0 and the Rayleigh range Z_R. The beam optical diameter (d/A) is normalized by the aperture beam size d_0. The effective optical distance (B/A) is normalized by the Rayleigh range, and the resulting parameter is the reciprocal of the propagation Fresnel number N, given by Eq. (4). The near field $1/N$, varying from zero to one, is the Fresnel region, and the far field is the Fraunhofer region $(1/N$ large). Figure 8 gives a clear picture of the impact of the laser-induced beam curvature f_0 on propagation. In particular, the determination of beam quality relative to ideal and the beam Rayleigh range are strongly influenced by the induced wavefront. Also notice that at the beam aperture or image plane $(B/A=0)$, the beam-induced wavefront does not affect the beam diameter, as shown in Eq. (20) for $B=0$, which defines the location of the image. But it does affect the diameter and location of the beam waist. This effect is expected, because imaging a beam results in just magnification of the beam.

Rewriting Eq. (20) with unknown coefficients gives:

$$(d/A)^2 = a_0 + a_1(B/A) + a_2(B/A)^2, \tag{21}$$

where

$$d_0 = (a_0)^{1/2}, \tag{22}$$

$$f_0 = -2a_0/a_1, \tag{23}$$

$$Z_R = \{a_0/[a_2 - (d_0/f_0)^2]\}^{1/2}. \quad (24)$$

If a_1 is not equal to zero, the waist of the laser beam is not at the laser aperture. The location and diameter of the laser waist is given by Eqs. (25) and (26), respectively. At the waist the optical magnification of the beam is $A=1$, because in propagation from the exit aperture to the waist there are no intervening optics, giving an *ABCD* array of $[1, L/n; 0, 1]$.

$$d_w = [a_0 - a_1^2/(4a_2)]^{1/2}, \quad (25)$$

and

$$B_w = -a_1/(2a_2). \quad (26)$$

By taking Plexiglas™ burns at judiciously placed locations along the optical train, those for which the ratio B/A takes on a wide range of values in the near and far fields, we can predict an approximate beam size of a non-Gaussian laser beam at a given B/A. The division of the effective diameter d by the geometric magnification A at a location defined by the chosen B/A gives the effect of diffraction spreading of the beam. The ratio B/A is the optical distance. It is the effective distance B scaled by the magnification A. A nonzero value of the coefficient a_1 indicates that the initial beam is not recollimated, i.e., f_0 has an initial curvature as given by Eq. (23). If it were, Eq. (21) would produce a curve symmetric about the origin/image plane where $B=0$.

2.1 *Application of Theory*

The coefficients of Eq. (21) can be determined by a least-squares fit to data generated from laser burn patterns. A series of laser burn samples were made to determine the beam characteristics from a UTIL 14-kW laser, model number SN 1102 with $M=2$ unstable optical cavity, with all mirrors in the system internally water-cooled to control thermal lensing. The water-cooled mirrors in UTIL lasers are made by SPAWR Industries (Lake Havasu City, Arizona) and are "designed to accept cw laser beams of 3 KW/cm^2 with λ/20 thermal distortion at 10.6 μm."[7] The objective of the tests was to determine the best location of the recollimating mirror to allow the beam to be delivered to a laser work station up to 15 m from the laser platform within the beam diameter limits of the delivery duct. The laser burn time on the Plexiglas™ test pieces was chosen to determine the perceived maximum beam size during propagation. The maximum beam diameters used in this analysis were not chosen using the method developed in the first section of this work. Instead, the data were selected on the judgment and experience of the engineer running the test to determine at what burn time the change in burn diameter was perceived to encircle 99% of the power. In other words, at what burn time the change in beam diameter started to be minimal.

A schematic of the UTIL laser optics path to the test stations is shown in Fig. 9. The laser beam is focused by mirror f_1 to allow the beam to exit the laser cavity through the aerodynamic window and then be recollimated at mirror f_2. At the recollimating station, the mirror can be moved up (−) or down (+) to control the beam diameter at the work station up to 15 m from the laser platform. The mirror focal

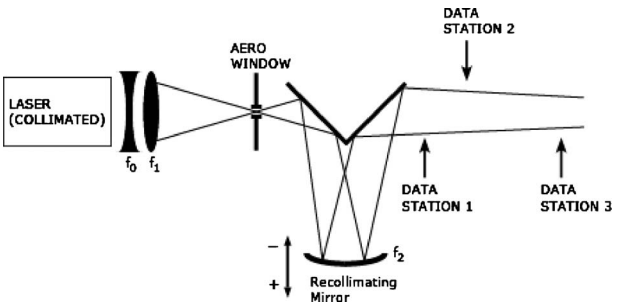

Fig. 9 UTIL Laser optical path model.

lengths and their contributions to the system *ABCD* array from the laser aperture to the collimator mirror and from the collimator mirror to the exit from the laser platform at the top of the laser cabinet are listed in Table 2.

Data are shown for three locations of the recollimator mirror f_2 that in this series of tests was offset from zero by lowering the mirror 15.24 cm (6 in.) and 22.86 cm (9 in.), respectively. Also shown in Table 2 are the distance from the recollimator mirror to the beam exit at the top of the laser platform, and the distance to the image plane. The image plane location ($B=0$) varies from 2 to 2.5 m from the laser platform, depending on the recollimator offset.

Tables 3–5 show the build-up of the *ABCD* array for the 11 data points in this test series from the laser platform to the test stations, and the regression data points in rows *X* and *Y*, followed by the test and estimated value of $(d/A)^2$ and d/A. Finally, the test and estimated values of the beam diameters show a standard deviation error in predicting the beam diameter of 2.7 mm.

The water-cooled mirrors in UTIL lasers are manufactured by Spawr Industries. Designed UTIL experience has shown that thermal lensing of the mirrors has been controlled by the use of internally cooled mirrors.[7] This ther-

Table 2 UTIL laser optics path from the laser aperture to the exit from the laser platform Laser: SN 1102; hole coupler=1 in.; cavity optics: $M=2$; and power level=14 kW.

Recollimator offset, δ (cm/in.)	0/0	15.24/6	22.86/9
f_1 (cm)	241.3	241.3	241.3
f_2 (cm)	241.3	241.3	241.3
$L_0=B_0=f_1+f_2+\delta$ (cm)	482.6	497.84	505.46
A_0	−1.00	−1.06	−1.09
C_0 (1/cm)	0.00E+00	2.62E−04	3.93E−04
$D_0=D$	−1.00	−1.06	−1.09
$A_0D_0-C_0B_0$	1	1	1
Recollimator distance to the exit of the laser platform (m)	2.32	2.48	2.55
Distance to image plane from laser platform ($B=0$), L_i (m)	2.51	2.2	2.07

Table 3 Laser test data analysis for zero collimator mirror offset.

Distance from recollimator (m)	2.42	4.76	17.56
Distance from platform to test station (m)	0.09	2.44	15.24
A	−1.00	−1.00	−1.00
B (m)	2.41	0.06	−12.74
$X=B/A$ (m)	−2.41	−0.06	12.74
d/A test (mm)	−54.0	−56.0	−80.0
$Y=(d/A)^2$ test (mm^2)	2916	3136	6400
$(d/A)^2$ estimate (mm^2)	3064	3315	7624
d/A estimate (mm)	55.4	57.6	87.3
Beam diameter test d (mm)	54.0	56.0	80.0
Beam diameter estimate d (mm)	55.4	57.6	87.3
Diameter error (mm)	1.4	1.6	7.3

mal lensing stability is required to ensure accurate and repeatable performance for industrial applications operating around the clock. Therefore, the burn data in Tables 3–5 can be combined into one dataset for regression analysis.

Table 6 shows the results of the regression analysis with a correlation coefficients r^2 for Eq. (20) of 0.996, and each of the three correlation coefficients passing statistical

Table 4 Laser test data analysis for recollimator mirror offset of $\delta=15.24$ cm.

Distance from recollimator mirror (m)	2.58	4.91	9.49	17.72
Distance from laser platform to test station (m)	0.10	2.44	7.01	15.24
A	−1.0	−0.93	−0.81	−0.60
B (m)	2.24	−0.25	−5.11	−13.86
$X=B/A$ (m)	−2.25	0.26	6.27	23.12
d/A test (mm)	−55.2	−58.9	−72.4	−123.4
$Y=(d/A)^2$ test (mm^2)	3051	3464	5243	15239
$(d/A)^2$ estimate (mm^2)	3076	3363	4825	14764
d/A estimate (mm)	55.5	58.0	69.5	121.5
Beam diameter test d (mm)	55.0	55.0	59.0	74.0
Beam diameter estimate d (mm)	55.2	54.2	56.6	72.8
Diameter error (mm)	0.2	−0.8	−2.4	−1.2

Table 5 Laser test data analysis for recollimator mirror offset of $\delta=22.86$ cm.

Distance from recollimator mirror (m)	2.65	4.99	9.56	17.79
Distance from laser platform to test station (m)	0.10	2.44	7.01	15.24
A	−0.99	−0.90	−0.72	−0.40
B (m)	2.15	−0.41	−5.41	−14.42
$X=B/A$ (m)	−2.14	0.46	7.53	36.41
d/A test (mm)	−55.5	−59.0	−76.5	−169.1
$Y=(d/A)^2$ (mm^2)	3083	3477	5847	2,8600
$(d/A)^2$ estimate (mm^2)	3082	3393	5270	2,8678
d/A estimate (mm)	55.5	58.3	72.6	169.3
Beam diameter test d (mm)	55.0	53.0	55.0	67.0
Beam diameter estimate d	55.0	52.4	52.2	67.1
Diameter error (mm)	0.0	−0.6	−2.8	0.1

t-critical of 3.36 and F-critical of 17.2 tests at a probability of 0.01. Table 7 details the laser characteristics such as beam diameter at the waist and aperture, respectively, d_w of 54.6 mm and d_0 of 57.7 mm at the aperture, beam curvature f_0 of −46.1 m, and Rayleigh range Z_R of 15.6 m. The spreading angle due the cavity-induced curvature is −1.25 mrad with a diffraction angle of 3.69 mrad, giving an overall spread angle of 3.89 mrad.

Figure 10 shows the variation of test data (d/A) versus propagation distance (B/A) compared to the derived correlation function (solid line). The correlation function is an excellent fit to the data and demonstrates that the data from

Table 6 Regression analysis summary.

	a_0	a_1	a_2
Coefficients	3,324	144.39	15.16
Std error of coefficients	193.27	40.48	1.24
Std Err of Y estimate	537.11		
r^2	0.996		
Degrees of Freedom	8		
F	1080		
F-critical	8.65		
t-coefficients	17.20	3.57	12.23
t-critical	3.36		

Table 7 Summary of test laser characteristics.

Beam diameter at waist d_w (mm)	54.59
Beam aperture diameter d_0 (mm)	57.66
Beam induced curvature f_0 (m)	–46.05
Rayleigh range Z_R (m)	15.64
Spreading angle d_0/f_0 (mrad)	–1.25
Diffraction spread angle d_0/Z_R (mrad)	3.69
Overall spread angle (mrad)	3.89

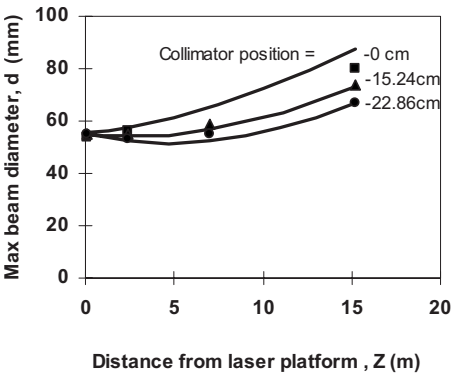

Fig. 11 Laser beam diameter correlation vs. propagation distance. Kecollimator offset ■=0 cm, ▲=15.24, ●=22.86 cm.

different optical configurations can be correlated to retrieve the fundamental laser beam characteristics d_0, f_0, and Z_R. The data cover the full range of conditions from the beam aperture and image point $(B/A=0)$ to well into the far field. The fact that optical diameter d/A continues to decrease in the negative B/A range reflects the negative curvature induced by the laser cavity. The waist of the beam occurs at B/A of −4.76 m with d/A of 54.6 mm. If the minimum optical beam diameter was a minimum in the positive B/A range, this would reflect a positive induced curvature by the laser cavity.

Figure 11 shows the beam diameter versus propagation distance from the recollimator cabinet. The solid lines are the calculated results from the correlation equation. Again, the correlation equation replicates the test data quite well.

The correlation demonstrates that the beam propagation assumption of an embedded Gaussian in the beam from an actual unstable laser resonator is reasonable, and that *ABCD* optical path matrix gives an accurate picture of the beam size during propagation. The correlation also demonstrates that using the *ABCD* optical path matrix allows the data from multiple optical configurations to be combined into a single dataset to analyze the laser beam propagation properties. Also of interest is the similarity of the laser beam curvatures of Figs. 8 and 11, reinforcing the ability of this method to determine fundamental laser beam propagation characteristics.

In addition, this method gives primary information on beam aperture diameter, cavity-induced curvature, and Rayleigh range. In combination with the analysis in the first section of the work, this analysis allows for the design of an optical system to keep the encircled power within the limits for a high power laser transfer system. Finally, an *ABCD* analysis using T and R as defined before to model the optical train would help in the selection and positioning of the recollimating mirror to control the beam size into the workstation and focus head. An Excel spreadsheet program to optimize the optical system for a given laser application is available from Ref. 3.

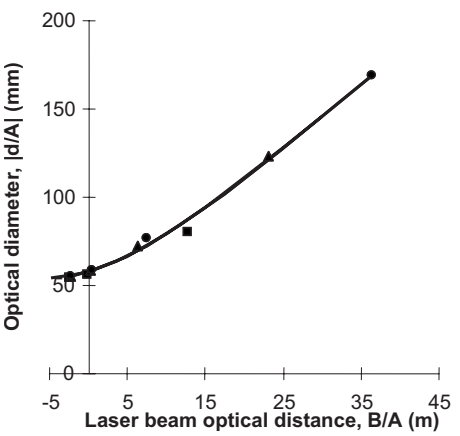

Fig. 10 Laser beam optical diameter vs. optical distance. Power =14 kW; cavity optics M=2; collimeter offset ■=0 cm, ▲=15.24 cm, ●=22.86 cm.

3 Beam Quality

Our analysis of laser burn patterns uses a wavelength multiplier to quantify the laser beam quality. This parameter includes the effects of all beam quality degradation effects. Some degradation effects are identifiable, some are not. Some are correctable, some are not. For instance, to achieve a large mode volume, hence a high output power, UTIL uses an unstable resonator. As long as the equivalent Fresnel number is not too small, the beams are approximately geometric in size. Figure 12 shows the prototypical confocal unstable resonator design, which assumes cylindrical symmetry for discussion purposes.

The drawback is that now the beam has a hole in the center where the feedback beam is created. Assume we create the perfect beam defined to be geometric (very high Fresnel number). Using the traditional definition of beam quality β, where we measure the focal plane (equivalent to far field) power in a bucket of radius of $r=1(f\lambda/D)$, or

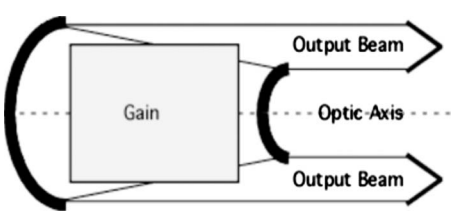

Fig. 12 Schematic of an unstable resonator laser.

sometimes $r=1.22(f\lambda/D)$, the location of the first zero in the Bessel function $J_1(x)$ for both the experimental beam and the ideal circular beam[8] gives:

$$\beta=\{[P_{\text{ideal}}(1f\lambda/D)]/[P_{\text{measured}}(1f\lambda/D)]\}^{1/2}\geqslant 1. \quad (27)$$

We find that our perfect beam does not have a beam quality of unity. Using a filled-in plane wave—in this case a circle—as the ideal beam, we see that due to geometric effects alone, our beam quality is degraded. However, if we define the ideal beam to be the annulus that matches the geometric output beam shape, we find that $\beta\approx 1$ for our perfect high-Fresnel-number beam.

Similarly, when designing a single-mode stable resonator, an output aperture can be sized to increase the higher order mode loss while minimizing the effect on the fundamental Gaussian mode. However, this aperture does diffract some of the fundamental mode, so it will degrade the beam quality somewhat. Again, the degradation is on purpose. For the unstable resonator, it was to increase the output power. For the stable resonator, it was to eliminate unwanted modes. When comparing a stable resonator mode to perfect, perfect should include the effects of the mode-selection aperture.

Other effects can also be identified as quality degradation sources: internal apertures, internal medium nonlinear profiles, mirrors aberrated due to local intensity and overall power absorption, thermal blooming, turbulence, etc. Depending on where your burn patterns are taken, these effects can also occur external to the cavity. To minimize your beam's actual beam quality, you should correct as many unwanted sources of degradation as possible. For example, if the gain medium generates tilt in the beam, tilt a nearby mirror to correct for it. Note that the resonator mode is the result of many roundtrips of the beam through the cavity, so the best correction is probably more easily determined running a computer simulation of the resonator. If the gain spatial distribution can be approximated by a mathematical function, you could manufacture a shape-correcting mirror, typical of the adaptive optics mirrors used for thermal blooming.

In summary, in some sources of aberration/degradation you can correct and some you cannot or choose not to due to cost. The wavelength multiplier found in this work includes all effects on the beam, both intentional and nonintentional. We refer to this multiplier as the beam quality. To determine its relationship to a beam quality number, you must first decide what constitutes the ideal beam used as the comparison baseline. A similar discussion holds for the definition of the Strehl intensity (the on-axis intensity relative to that of the "perfect" beam).

The beam quality of the test laser beam can be estimated from the laser beam propagation analysis characteristics developed from the laser images burned into the Plexiglas™ test samples. The propagation analysis assumes an embedded Gaussian in the laser beam, requiring the Fresnel number and Rayleigh range of the laser beam and Gaussian to be equal [see Eq. (4)]. The laser beam propagation analysis demonstrated that from data that covers a wide range of Fresnel numbers from the near field to the far field, the fundamental properties of the laser beam can be determined. These include the laser cavity-induced curvature, aperture beam size, and Rayleigh range size and Rayleigh range, as given in Eqs. (21) and (23), respectively. The Rayleigh range found is actually the effective Rayleigh range, which takes into account the imperfect nature of the laser beam. Typically, the effect is taken into account by using wavelength scaling,

$$\lambda_e=\beta\lambda, \quad (28)$$

where β is the beam quality and is measured in the far field to be the square root of the ratio of the ideal power to the actual power contained in the far-field spot size, as defined in Eq. (27). The Rayleigh range, defined in Ref. 4 page 668, for a Gaussian and laser beam is given by:

$$Z_R\equiv\pi\omega_0^2/\lambda_e=r_w^2/\lambda_e=r_w^2/(\beta\lambda), \quad (29)$$

where ω_0 is the embedded Gaussian beam size at the waist, r_w is the laser beam waist size, and λ_e is the effective beam wavelength. Therefore, Eq. (29) can be rewritten to define this effective wavelength, hence the beam quality, as:

$$\beta=(\pi\omega_0^2)/(\lambda Z_R)=r_w^2/(\lambda Z_R)=(d_w/2)^2/(\lambda Z_R). \quad (30)$$

Similarly, the laser beam propagation factor M^2 defined by Eq. (18) in Johnston[9] is given by:

$$M^2=(\pi\omega_0^2)/(\lambda Z_R). \quad (31)$$

Therefore, β and M^2 are numerically equivalent in describing the diffraction of laser beam due to the reduction in the Rayleigh range relative to the ideal.

Using the laser characteristics data from Table 7 with the beam waist d_w of 54.6 mm gives a beam quality number of 4.5 for the UTIL 2 Mod SN 1102 laser running at 14 kW. This beam quality number includes the effects of the laser cavity refraction as well as the diffraction due to the laser beam aperture and diffraction due to the aerodynamic window.

4 Summary

This work demonstrates a fairly accurate, robust, and very inexpensive way to determine experimentally the propagation characteristics of laser beams for both stable and unstable laser resonators. The work demonstrates that the primary characteristics of a laser beam can be determined from Plexiglas™ burn samples. The linear relationship between the weight loss in the Plexiglas™ and laser burn time (see Fig. 3) indicates that the extent of the burn pattern and amount of energy absorbed by the Plexiglas™ is limited by the laser energy density threshold (J/cm^2) required to vaporize the Plexiglas™. Therefore, the burn time required at a given laser power to initiate vaporization is dependent on the peak irradiance of the laser beam. At longer burn times, the extent of the burn pattern increases to the density limit. The total energy absorbed by the Plexiglas™ is proportional to the size of the burn pattern. The exponential function [see Eq. (9)] developed to model the extent of the burn pattern defines three important characteristics of the laser beam at a particular test station. These are the burn time to initiate vaporization (t_0), the beam size (d_s), and the tail of the laser irradiance profile to allow prediction of the maximum beam diameter (99% of beam power) [see Eq. (13)].

This allows an approximation of the laser irradiance profile I_r/I_0 and peak power irradiance I_0 to be determined by Eqs. (10) and (11), respectively. The laser irradiance profile for the test laser is shown in Fig. 6. The encircled power of the test laser is given by Eq. (12) and compared to the embedded Gaussian beam in Fig. 7.

Laser beam propagation analysis assumes an embedded Gaussian that is propagated through the laser *ABCD* optical path matrix. Using the *ABCD* optics matrix allows the data from different optical configurations to be combined into a single dataset to determine the beam propagation characteristics. The resultant quadratic equation [see Eq. (20)] solved for the beam optical diameter (d/A) as a function of the beam optical distance (B/A) as primary variables. Using Eq. (20), a regression analysis of laser beam optical path data defines the primary laser beam characteristics. The three characteristics defined are the beam diameter (d_0) at the laser output aperture, the laser cavity-induced beam curvature (f_0), and the laser beam Rayleigh range (Z_R). In addition, if there is an induced beam curvature, the laser beam waist diameter d_w and location B_w can be determined by Eqs. (25) and (26), respectively. The results of the regression analysis on a UTIL 14-kW laser are demonstrated in Tables 3–5, and Figs. 10 and 11.

The beam quality of the laser is defined by assuming that the Rayleigh range and beam Fresnel number for the test laser and the embedded Gaussian beam are equal. Therefore, the beam quality β [Eq. (30)] is defined by the beam waist diameter d_w [Eq. (25)] and the Rayleigh range Z_R [Eq. (29)] and is used to define the effective wavelength λ_e [Eq. (28)]. The beam quality is simply the ratio of the effective and actual wavelengths.

References

1. J. W. Davis, J. P. Carstens, and E. W. Kehren, "History, current status and future prospects for laser technology at UTIL," presented at the Canadian Industrial Laser Association 1990 Conf, Laser Technology—Applications in Canadian Industry, Edmonton, Alberta, 18–19 April 1990.
2. S. S. Townsend and P. R. Cunningham, "Gaussian scaling laws for diffraction," in *Proc. SPIE* **1415**, 36 (1991).
3. S. S. Townsend, "Back of the envelope optical design," (unpublished manuscript).
4. "Real beam propagation," see http://www.mellesgriot.com/pdf/CatalogX/X_02_10-12.pdf, file format PDF/Adobe Acrobat, Quick View for a true Gaussian beam, M2=1. EMBEDDED GAUSSIAN (the concept of an "embedded Gaussian," shown in Fig. 2.15, is useful as a construct to assist).
5. A. E. Siegman, *Lasers*, University Science Books, Mill Valley, CA (1986).
6. A. E. Siegman, "Defining the effective radius of curvature for a non-ideal optical beam," *IEEE J. Quantum Electron.* **27**, 1146–1148 (May 1991).
7. See http://www.spawrindustries.com, SPAWR Industries, Inc., Lake Havasu City, AZ 86403.
8. T. S. Ross and W. P. Latham, "Appropriate measures and consistent standard for high energy laser beam quality (postprint)," *J. Direct Energy* **2**, 22–58 (2006).
9. T. F. Johnston, "Beam propagation (M^2) measurement made as easy as it gets: the four-cuts method," *Appl. Opt.* **37**, 4840–4850 (July 1998).

John S. Foley is a retired engineer from United Technologies Industrial Lasers (UTIL), where he was the manager of market development. He earned a BAE from New York University in aeronautical engineering. He worked for United Technologies Research Center (UTRC) in the systems analysis group simulating and computer modeling the impact of advances in aerodynamics and structures on the design, performance, weight, and cost of commercial and military aircraft for subsonic and supersonic applications. He also analyzed wind turbine design, performance, and costs for wind systems designed for small applications and multimegawatt wind farms. He transferred from the system analysis group to the laser group at UTRC before UTIL became a division of the United Technologies Corporation. He has a patent on "Laser pipe welding systems for nonstationary pipe."

Sallie S. Townsend is an optical physicist who earned her PhD in room-temperature quantum mechanics at the University of New Hampshire. She then worked for United Technologies performing design, analysis, simulation, and computer modeling of high-energy lasers and optical systems. After leaving United Technologies, she formed a small, small business innovation research (SBIR)-funded laser business, in which she and her business partner industrialized a laboratory scale photolytic iodine laser. Her industrial work has led to six patents, the latest patent being for a spherical shell laser that uses imaging of an effective point source instead of focusing a collimated beam. For the last 13 years she has taught mathematics and physics at the University of Hartford. Her current research interests include the visualization of the equations of motion of dynamical systems using Adobe Flash.